Available online at www.sciencedirect.com
SCIENCE DIRECT®
Journal of Solid State Chemistry 177 (2004) 2249–2254
JOURNAL OF SOLID STATE CHEMISTRY
http://elsevier.com/locate/jssc

# Crystal and electronic structure of the red semiconductor $Ba_4LaSbGe_3Se_{13}$ comprising the complex anion $[Ge_2Se_7-Sb_2Se_4-Ge_2Se_7]^{14-}$

Abdeljalil Assoud, Navid Soheilnia, and Holger Kleinke*

*Department of Chemistry, University of Waterloo, 200 University Ave. W., Waterloo, Ontario, Canada N2L 3G1*

Received 7 January 2004; received in revised form 23 February 2004; accepted 7 March 2004

**Abstract**

$Ba_4LaGe_3SbSe_{13}$ was prepared by reacting the elements under exclusion of air at 700°C, followed by slow cooling to room temperature. It crystallizes in a new type of the monoclinic space group $P2_1/c$, with lattice dimensions of $a = 1633.30(9)$ pm, $b = 1251.15(7)$ pm, $c = 1303.21(7)$ pm, $\beta = 103.457(2)^\circ$, $V = 2590.0(2)\ 10^6\ pm^3$ ($Z = 4$). The structure contains isolated $GeSe_4$ as well as $Ge_2Se_7$ digermanate units. Two of the latter are interconnected via an $Sb_2Se_4$ bridge yielding an almost linear complex anion $[Ge_2Se_7–Sb_2Se_4–Ge_2Se_7]^{14-}$. The oxidation states are assigned to be $Ba^{II}$, $La^{III}$, $Ge^{IV}$, $Sb^{III}$, and $Se^{-II}$, in accord with an electronically saturated nonmetal. The lone pair of $Sb^{III}$ reflects itself in highly irregular Se coordination. The red color of the material is indicative of semiconducting behavior with an activation energy of 2.0 eV. Electronic structure calculations based on the LMTO approximation point to a smaller gap, typical for this calculation method. We utilized the COHP tool to explore the bonding character of the different Sb–Se interactions.


*Keywords:* Crystal structure; Electronic structure; Semiconductor; Germanium; Antimony; Selenium

## 1. Introduction

Among the most studied materials in thermoelectric research are ternary and higher antimony chalcogenides [1–10], bismuth chalcogenides [11–15], and germanium and tin-based clathrates [16–19]. A particularly well explored family of high-temperature thermoelectrics is $(AgSbTe_2)_{1-x}(GeTe)_x$ (TAGS) [20,21]. Based on this, we are currently investigating higher germanium antimony chalcogenides.

While there are no analogous selenides known that comprise both Ge and Sb, a handful of seleno-germanates as well as seleno-antimonates have been reported before. The former are often noncentrosymmetric and typically exhibit $Ge^{IV}Se_4$ tetrahedra (e.g., $Sr_2GeSe_4$ [22], $KLaGeSe_4$ [23], $K_2Hg_3Ge_2Se_8$ [24]), but trivalent ($Sr_2Ge_2Se_5$) and divalent Ge selenides ($Ba_2Ge_2Se_5$) are known as well [25]. Much more seleno-antimonates exist, which typically show irregular Se coordination of the $Sb^{III}$ atoms [2,26], comparable to $Sb_2Se_3$ [27]. Arguably the compound most comparable to the title compound $Ba_4LaGe_3SbSe_{13}$ is the noncentrosymmetric quaternary silicon antimony selenide $Ba_4SiSb_2Se_{11}$ [28] that shows only little structural resemblance, if any.

## 2. Experimental

### 2.1. Synthesis and analysis

We synthesized $Ba_4LaGe_3SbSe_{13}$ by heating the elements in an evacuated silica tube between 700°C and 800°C. In the initial attempt, we chose the four cationic elements in the equiatomic ratio, and added six equivalents of selenium to achieve the common oxidation states ($Ba^{II}$, $La^{III}$, $Ge^{IV}$, $Sb^{III}$, $Se^{-II}$). After annealing the mixture at 800°C over a period of 1 week, the furnace was slowly cooled to room temperature with a cooling rate of 100°C/day. Next, the reaction mixture was analyzed by an X-ray powder diffractogram (INEL, with position-sensitive detector and Cu$K\alpha_1$ radiation). As no known compound could be identified, a red

*Corresponding author. Fax: +1-519-746-0435.
*E-mail address:* kleinke@uwaterloo.ca (H. Kleinke).

0022-4596/$ - see front matter © 2004 Elsevier Inc. All rights reserved.
doi:10.1016/j.jssc.2004.03.008

block-shaped single crystal was mounted for a room temperature data collection onto a Smart Apex CCD (BRUKER) for its single crystal structure determination. Data were collected by scans of 0.3° in $\omega$ at $\phi = 0°$ and 60°, for an overall of $2 \times 606$ frames, with an exposure time of 60 s per frame. The data were corrected for Lorentz and polarization effects. Absorption corrections were based on fitting a function to the empirical transmission surface as sampled by multiple equivalent measurements [29]. The unit cell parameters were readily obtained by indexing the diffraction peaks obtained from all frames of the reciprocal space images. The matrix indicated primitive monoclinic symmetry, and the systematic absences of $k = 2n + 1$ for all $0\,k\,0$ and $l = 2n + 1$ for all $h\,0\,l$ reflections are unambiguously in agreement with the space group $P2_1/c$ (No. 14).

Employing the direct methods we obtained a reasonable structure solution in this space group without any interatomic distances shorter than 230 pm. The assignments of atoms to the peaks obtained was straightforward based on their coordination spheres and intensities, noting that the distances to the Se atoms are supposed to increase substantially from Ge to Sb to La to Ba. The structure refinements [30] of the structure model with the formula $Ba_4LaGe_3SbSe_{13}$ converged smoothly to satisfying residual factors. Crystallographic details are given in Table 1, atomic positions and equivalent displacement parameters in Table 2. Further details of the crystal structure investigation can be obtained from the Fachinformationszentrum Karlsruhe, 76344 Eggenstein-Leopoldshafen, Germany, (fax: (49) 7247-808-666; e-mail: crysdata@fiz-karlsruhe.de) on quoting the depository number CSD-413611.

Table 1
Crystallographic data of $Ba_4LaGe_3SbSe_{13}$

| | |
|---|---|
| Chemical formula, formula weight (g/mol) | $Ba_4LaGe_3SbSe_{13}$, 2054.27 |
| $T$ (K), $\lambda$ (pm) of measurement | 295, 71.073 |
| Crystal size (μm) | $80 \times 70 \times 60$ |
| space group, $Z$ | $P2_1/c$, 4 |
| $a$ (pm) | 1633.30(9) |
| $b$ (pm) | 1251.15(7) |
| $c$ (pm) | 1303.21(7) |
| $\beta$ (deg) | 103.457(2) |
| $V$ ($10^6$ pm$^3$) | 2590.0(2) |
| $\mu$ (mm$^{-1}$) | 30.30 |
| $F(000)$ | 3480 |
| $\rho_{calcd}$ [g/cm$^3$] | 5.27 |
| $\theta$ range for data collection | $2.1 < \theta < 35.0°$ |
| Reflections collected; independent ($R_{int}$) | 27886; 10897 (6.27%) |
| Observed reflections; parameters | 8332; 200 |
| Refinement method | Full-matrix least-squares on $F^2$ |
| Goodness-of-fit on $F^2$ | 1.13 |
| $R(F_o)$; $R_w(F_o^2)$ with $I > 2\sigma(I)$ | 0.070; 0.095 |
| Extinction coefficient | 0.00010(1) |
| Effective min. transmission | 0.64 |
| Largest diff. peak; hole ($e$/($10^6$ pm$^3$)) | 3.35; −2.36 |

Table 2
Atomic coordinates and equivalent displacement parameters

| Atom | $x$ | $y$ | $z$ | $U_{eq}$ (Å$^2$) |
|---|---|---|---|---|
| Ba(1) | 0.05228(4) | 0.67662(5) | 0.45475(5) | 0.01402(13) |
| Ba(2) | 0.15260(4) | 0.17339(5) | 0.35270(5) | 0.01485(13) |
| Ba(3) | 0.36448(4) | 0.31599(5) | 0.15575(5) | 0.01481(13) |
| Ba(4) | 0.25696(5) | 0.83067(5) | 0.27105(5) | 0.01774(14) |
| La(1) | 0.35627(4) | 0.52202(5) | 0.45243(5) | 0.01015(11) |
| Ge(1) | 0.18106(7) | 0.09047(8) | 0.07794(9) | 0.0102(2) |
| Ge(2) | 0.33041(7) | 0.61745(8) | 0.07682(9) | 0.0109(2) |
| Ge(3) | 0.48473(7) | 0.26684(9) | 0.43823(9) | 0.0107(2) |
| Sb(1) | 0.08036(5) | 0.51804(6) | 0.13583(6) | 0.01574(15) |
| Se(1) | 0.31952(7) | 0.05696(8) | 0.16503(8) | 0.0132(2) |
| Se(2) | 0.09050(7) | 0.99114(8) | 0.15889(9) | 0.0135(2) |
| Se(3) | 0.14934(7) | 0.27211(8) | 0.10234(9) | 0.0139(2) |
| Se(4) | 0.16144(7) | 0.45635(9) | 0.39947(8) | 0.0137(2) |
| Se(5) | 0.26960(7) | 0.55849(9) | 0.21482(8) | 0.0126(2) |
| Se(6) | 0.26184(7) | 0.78102(8) | 0.01605(9) | 0.0134(2) |
| Se(7) | 0.31951(7) | 0.01345(9) | 0.45028(9) | 0.0156(2) |
| Se(8) | 0.47886(7) | 0.62024(9) | 0.15343(9) | 0.0155(2) |
| Se(9) | 0.45168(7) | 0.72288(9) | 0.38446(8) | 0.0146(2) |
| Se(10) | 0.33671(7) | 0.28311(8) | 0.40718(8) | 0.0120(2) |
| Se(11) | 0.49664(7) | 0.93010(8) | 0.14368(8) | 0.0134(2) |
| Se(12) | 0.05329(7) | 0.70942(8) | 0.19222(9) | 0.0143(2) |
| Se(13) | 0.08394(7) | 0.94510(9) | 0.43986(9) | 0.0148(2) |

Following the successful structure solution, a new sample was prepared starting from the elements in the stoichiometric ratio. This sample was annealed at a lower temperature, namely at 700°C, for the first sample was molten at 800°C. All reflections of the powder diagram of this sample belonged to $Ba_4LaGe_3SbSe_{13}$, indicating quantitative yield. All our attempts to synthesize isotypic compounds failed, e.g., by replacing Ba with Sr, Ge with Si or Sn, or Sb with Bi.

Standardless energy dispersive spectroscopy (EDS, LEO 1050) was performed on the apparently phase-pure sample of $Ba_4LaGe_3SbSe_{13}$. No impurities of other elements (like silicon or oxygen stemming from the silica tube) were detected. Analyses of several selected crystals revealed high homogeneity. The averaged ratio of Ba:La:Ge:Sb:Se was 14:3.5:15:3.5:64 (in at%), while the ideal values based on the structure determination are 18.2:4.5:13.6:4.5:59.1. The quality of the analyses is impaired by the strong overlap of the Ba and La peaks and the small relative amount of both La and Sb, which is reflected in very small peaks of the latter two elements.

### 2.2. Physical property determinations

#### 2.2.1. Thermal analysis

We performed a temperature-dependent combined differential scanning calorimetry and thermogravimetry measurement with the computer controlled NETZSCH STA 409PC Luxx. The measurement was performed under a constant flow of Argon (30 mL/min), which also protected the balance (flow of 20 mL/min). Both the heating and the cooling rates were 20°C/min. The

temperature range was selected to be between room temperature and 720°C, to analyze whether a thermal effect (e.g., phase transformation or decomposition) would occur during the final cool-down procedure after annealing at 700°C. As no effect was observed, we conclude that $Ba_4LaGe_3SbSe_{13}$ is thermodynamically stable with respect to its neighboring phases under exclusion of air at least up to 720°C. Moreover, the melting point was not reached during the experiment.

#### 2.2.2. Resistivity measurement

We pressed part of the ground phase-pure sample into a bar-shaped pellet of the dimensions $5 \times 1 \times 1$ [in mm] for physical transport measurements, since no single crystals of sufficient dimensions were available. The high internal resistance of the pellet inhibited Seebeck and electrical conductivity measurements. We conclude based on our experiences with other high resistance materials that its specific resistance must be above 1 MΩ cm at room temperature.

#### 2.2.3. Electronic structure calculations

The self-consistent tight-binding *first principles* linear muffin tin orbitals (LMTO) method was utilized using the atomic spheres approximation (ASA) [31,32]. In the LMTO approach, the density functional theory is used with the local density approximation (LDA) [33]. The integration in $k$ space was performed by an improved tetrahedron method [34] on a grid of 252 independent $k$ points of the first Brillouin zone. We extracted the densities of states (DOS) from the band structure calculation, which in turn was weighed into its pairwise bonding and antibonding contributions, yielding the crystal orbital Hamilton population (COHP) [35]. The COHP curves resemble the well-established crystal orbital overlap population (COOP) curves [36] usually extracted from Extended Hückel calculations, where bonding interactions are depicted on the right side of the diagram, and antibonding ones on the left. Integrating over all filled states yields the ICOHP values, in analogy to the Mulliken overlap populations (MOP) [37] obtained from COOP curves. ICOHP values differ from MOP values in their sign (i.e., negative values indicate bonding character) and units (eV per bond vs. electrons per bond). As demonstrated before [38–40], the absolute ICOHP values are typically higher than the corresponding MOP values (ignoring the different units).

## 3. Results and discussion

### 3.1. Structure and bonding

$Ba_4LaGe_3SbSe_{13}$ crystallizes in a new structure type. As all lattice parameters are larger than 1250 pm, a full view of the unit cell is not very helpful in understanding the structure. In Fig. 1, we exclude we exclude the Ba–Se and La–Se bonds for clarity, showing all other bonds shorter than 310 pm. The $GeSe_4$ tetrahedra are depicted in a polyhedral representation.

Both the Ba and the La atoms are surrounded by eight Se atoms in rather irregular coordination spheres. The distances to the Se atoms are quite significantly different, ranging from 323 to 359 pm for the Ba–Se and from 303 to 320 pm for the La–Se distances. For details it is referred to Table 3. The values concur nicely with the differences in the ionic radii for eight-fold coordination, e.g., Pauling's ionic radii [41] for $Ba^{2+}$: 135 pm, and for $La^{3+}$: 115 pm. The bond lengths are of the order of the sum of the ionic radii of 333 and 313 pm, respectively (using Pauling's value of 198 pm for $Se^{2-}$).

Compared to the Ba–Se and La–Se bonds, the Ge–Se and Sb–Se interactions are expected to be highly covalent. All three symmetry independent Ge sites are coordinated by four Se atoms at distances between 232 and 240 pm, forming distorted 'tetrahedra' (bond angles between 95° and 119°). Such distances (as well as the tetrahedral coordination) are within the normal range of bonds between tetravalent Ge and Se; e.g., α-$GeSe_2$ comprises bonds of 234–237 pm [42].

One of the three independent tetrahedra, centered by Ge(1), is not connected to the others (isolated tetrahedron), while the two others form $Ge_2Se_7$ pairs via corner-sharing. Between two of the latter pairs we find a centrosymmetric $Sb_2Se_4$ unit, which is bonded to one Se per $Ge_2Se_7$ unit via a longer Sb–Se contact of 306 pm, compared to the three short Sb–Se bonds of 257–279 pm within the $Sb_2Se_4$ unit. The Se atoms of the $Ge(1)Se_4$ tetrahedra are further apart from the $Sb_2Se_4$ unit, namely 334 and 347 pm (Fig. 2). As the sum of Pauling's single bond radii of Sb and Se is 256 pm, the bonding character of Sb–Se contacts larger than 300 pm is either weak, or nonexistent.

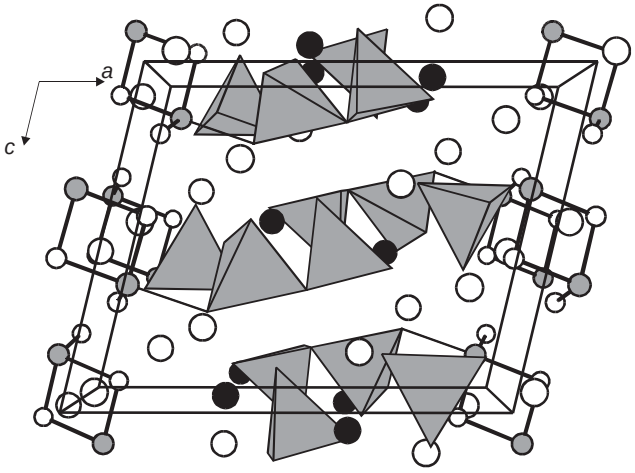


Fig. 1. Structure of $Ba_4LaGe_3SbSe_{13}$ in a projection along [010]. Large white circles: Ba; black: La; gray: Sb; small, white: Se. $GeSe_4$ tetrahedra are shown as gray polyhedra.

Table 3
Selected interatomic distances (pm)

| | | | |
|---|---|---|---|
| Ba(1)–Se(2) | 333.17(13) | Ba(2)–Se(10) | 323.07(12) |
| Ba(1)–Se(6) | 337.08(13) | Ba(2)–Se(12) | 330.74(13) |
| Ba(1)–Se(2) | 337.77(13) | Ba(2)–Se(3) | 333.66(13) |
| Ba(1)–Se(12) | 340.39(13) | Ba(2)–Se(13) | 336.14(13) |
| Ba(1)–Se(13) | 341.10(13) | Ba(2)–Se(2) | 337.87(13) |
| Ba(1)–Se(3) | 341.83(13) | Ba(2)–Se(7) | 338.22(13) |
| Ba(1)–Se(4) | 344.83(13) | Ba(2)–Se(3) | 347.75(13) |
| Ba(1)–Se(12) | 344.97(13) | Ba(2)–Se(4) | 358.96(13) |
| | | | |
| Ba(3)–Se(1) | 333.14(12) | Ba(4)–Se(7) | 325.86(13) |
| Ba(3)–Se(11) | 335.50(12) | Ba(4)–Se(6) | 340.00(13) |
| Ba(3)–Se(7) | 336.87(13) | Ba(4)–Se(1) | 340.97(13) |
| Ba(3)–Se(9) | 337.34(13) | Ba(4)–Se(2) | 342.20(13) |
| Ba(3)–Se(10) | 339.89(13) | Ba(4)–Se(9) | 345.40(13) |
| Ba(3)–Se(10) | 343.57(13) | Ba(4)–Se(6) | 346.91(13) |
| Ba(3)–Se(3) | 346.33(13) | Ba(4)–Se(5) | 349.95(13) |
| Ba(3)–Se(5) | 357.15(13) | Ba(4)–Se(12) | 358.21(13) |
| | | | |
| La(1)–Se(11) | 302.79(12) | Sb(1)–Se(12) | 257.30(13) |
| La(1)–Se(10) | 304.91(12) | Sb(1)–Se(13) | 260.93(14) |
| La(1)–Se(6) | 311.99(12) | Sb(1)–Se(13) | 278.85(14) |
| La(1)–Se(5) | 312.42(12) | Sb(1)–Se(5) | 306.39(13) |
| La(1)–Se(1) | 312.84(12) | | |
| La(1)–Se(11) | 317.23(13) | Ge(1)–Se(1) | 232.02(15) |
| La(1)–Se(9) | 318.92(13) | Ge(1)–Se(2) | 236.05(15) |
| La(1)–Se(4) | 320.23(13) | Ge(1)–Se(3) | 236.87(15) |
| | | Ge(1)–Se(4) | 234.69(15) |
| Ge(2)–Se(5) | 236.57(15) | | |
| Ge(2)–Se(6) | 237.84(15) | Ge(3)–Se(8) | 233.99(15) |
| Ge(2)–Se(7) | 230.15(15) | Ge(3)–Se(9) | 230.60(15) |
| Ge(2)–Se(8) | 239.80(16) | Ge(3)–Se(10) | 236.53(16) |
| | | Ge(3)–Se(11) | 235.69(15) |

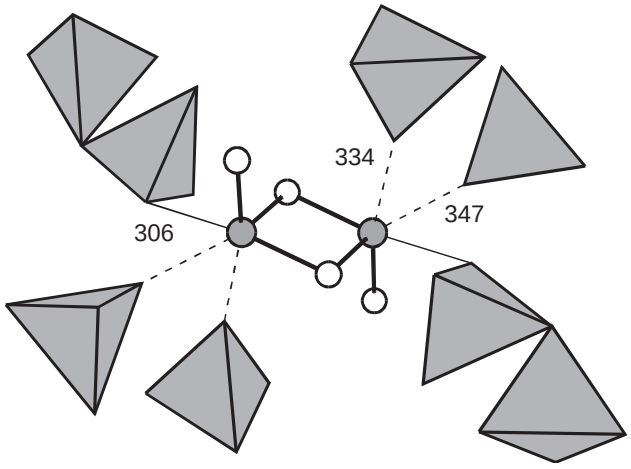


Fig. 2. Connection of the $Sb_2Se_4$ unit with the $GeSe_4$ tetrahedra and the $Ge_2Se_7$ double tetrahedra. Gray circles: Sb; white: Se. $GeSe_4$ tetrahedra are shown as gray polyhedra. The numbers displayed are the distances given in pm.

Overall, there are three Sb–Se bonds $<280$ pm per Sb atom, and three longer contacts between 306 and 347 pm. Roughly one can describe the polyhedron starting from an octahedron, and then elongating the distances of one triangular face to the Sb atom. This is likely a consequence of the sterically active inert pair of the $Sb^{III}$. Two of these $SbSe_6$ 'octahedra' share a common edge, yielding the $Sb_2Se_{10}$ unit depicted in Fig. 3. The resemblance to the $Sb_2Se_3$ structure is strong; in the binary, one Sb atom participates in three short bonds of 266–268 pm, and in three larger bonds of 322–325 pm. The second Sb atom of $Sb_2Se_3$ exhibits a more distorted Se coordination, like the Sb atom in $Ba_4LaGe_3SbSe_{13}$, with distances of 259, $2\times280$, $2\times301$, and $2\times349$ pm.

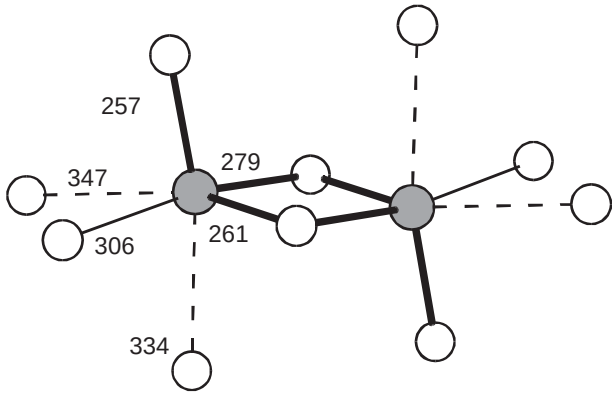


Fig. 3. The $Sb_2Se_{10}$ double 'octahedron'. Gray circles: Sb; white: Se. The numbers displayed are the distances given in pm.

We calculated the ICOHP values of these Sb–Se interactions, to verify whether or not the lengthier contacts are to be considered as bonding. The three bonds shorter than 280 pm comprise large ICOHP values between $-2.53$ and $-1.39$ eV/bond, and the 306 pm interaction $-0.34$. Therefore, while the last is undoubtedly much weaker than the shorter bonds, its bonding contribution is not negligible. On the other hand, the values for the contacts of 334 and 347 pm (dashed lines in Fig. 3) are almost zero ($-0.05$ and $-0.02$ eV/bond, respectively), so that they can be treated as nonbonding in a good approximation.

One can assess bond orders simply based on the different distances, assuming perfect bond length–bond strength correlations. The Pauling Bond orders [41] are calculated according to the formula

$$d(n) = d(1) + 60\ \text{pm}\log n,$$

with $d(n)$ = observed distance, $d(1)$ = single bond distance, and $n$ = Pauling bond order (PBO). With Pauling's single bond radii of 139 pm for Sb and 117 pm for Se, we obtain $d(1) = 256$ pm. Then, the shortest Sb–Se bond of $Ba_4LaGe_3SbSe_{13}$ (257 pm) is almost a single bond (PBO = 0.95), and the intermediate bond of 306 pm exhibits a PBO of 0.15. In this structure, there is a high correlation between the ICOHP and PBO values of all Sb–Se interactions, and therefore, a high bond length–bond strength correlation as well. The ICOHP values of Fig. 4 are divided by ICOHP(max) $= -2.53$ eV/bond to obtain dimensionless

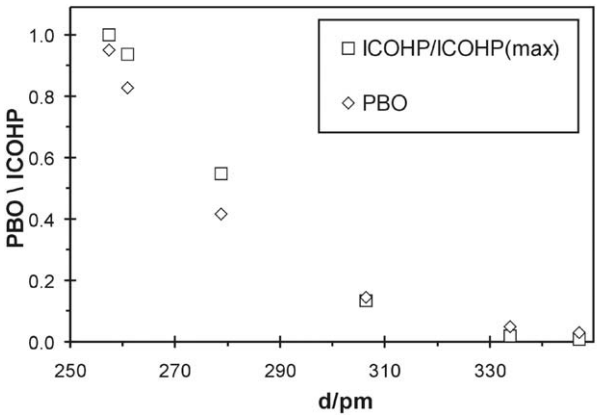


Fig. 4. Pauling bond orders (◇) and relative ICOHP values (□) for the Sb–Se interactions.

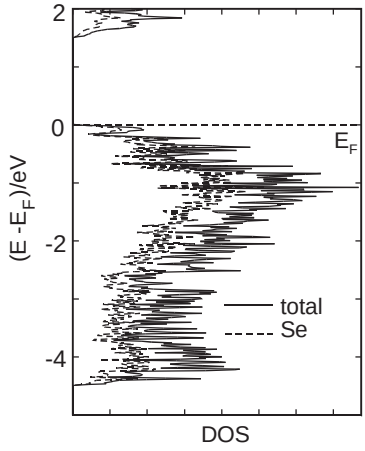


Fig. 5. Densities of states (DOS) for $Ba_4LaGe_3SbSe_{13}$. The Fermi level (dashed line) was arbitrarily placed at 0 eV.

values for comparison with the PBO values. Fig. 4 also illustrates that the Sb–Se distances larger than 330 pm cannot be regarded as bonding interactions.

Therefore, a detailed listing of the structure motifs includes $Ba^{2+}$ and $La^{3+}$ cations, tetrahedral anions $GeSe_4^{4-}$, and an almost linear isolated finite complex anion $[Ge_2Se_7–Sb_2Se_4–Ge_2Se_7]^{14-}$. There is no precedent for the latter motif; the most closely related chalcogenide $Ba_4SiSb_2Se_{11}$ [28] contains infinite $[SiSb_2Se_{11}]^{8-}$ chains consisting of isolated $SiSe_4$ tetrahedra sharing edges with square pyramidal $SbSe_5$ units.

### 3.2. Electronic structure and physical properties

$Ba_4LaGe_3SbSe_{13}$ is a red semiconducting material. Its DOS are shown in Fig. 5. The chosen energy window is dominated by the filled 4*p* states of Se that almost exclusively form the peak between 0 and −4.5 eV (i.e., the valence band), while the remaining states in that area stem from Ge and Sb states as a consequence of the covalent character of the Ge–Se and Sb–Se interactions. The calculated band gap of 1.5 eV is 25% smaller than expected for a red semiconductor (2.0 eV), [43] a discrepancy that is not atypical for local density approximations [44,45]. Above the gap, a large peak (i.e., the conduction band) starts that is comprised of a mixture of La *d*, Ba *s*, Ge *s*, and Sb *p* states. Again, the Se contributions to this peak result from covalent mixing.

## 4. Summary

The first mixed seleno-germanate/antimonate, $Ba_4LaGe_3SbSe_{13}$, was uncovered. Its structure is composed of $GeSe_4$ monotetrahedra and $Ge_2Se_7$ ditetrahedra. The latter are part of an almost linear unique anion of the composition $[Ge_2Se_7–Sb_2Se_4–Ge_2Se_7]^{14-}$, wherein weak Sb–Se interactions connect the central centrosymmetric $Sb_2Se_4$ unit to two $Ge_2Se_7$ ditetrahedra. The inert pair of the $Sb^{III}$ atom is sterically active, as reflected in a severely irregular Se coordination reminiscent of the situation in $Sb_2Se_3$. That $Ba_4LaGe_3SbSe_{13}$ is an electron-precise compound, according to the ionic formulation $(Ba^{2+})_4(La^{3+})(Ge^{4+})_3Sb^{3+}(Se^{2-})_{13}$, reflects itself in its red color.

## Acknowledgments

Financial support from NSERC, CFI, OIT (Ontario Distinguished Researcher Award for H.K.), the Province of Ontario (Premier's Research Excellence Award for H.K.) and the Canada Research Chair program (CRC for H.K.) is appreciated.

## References

[1] R. Venkatasubramanian, E. Slivola, T. Colpitts, B. O'Quinn, Nature 413 (2001) 597–602.
[2] J.H. Chen, P.K. Dorhout, J. Alloys Compd. 249 (1997) 199–205.
[3] K.-S. Choi, D.-Y. Chung, A. Mrotzek, P. Brazis, C.R. Kannewurf, C. Uher, W. Chen, T. Hogan, M.G. Kanatzidis, Chem. Mater. 13 (2001) 756–764.
[4] L.E. Shelimova, O.G. Karpinskii, P.P. Konstantinov, M.A. Kretova, E.S. Avilov, V.S. Zemskov, Inorg. Mater. 37 (2001) 342–348.
[5] T. Kyratsi, J.S. Dyck, W. Chen, D.-Y. Chung, C. Uher, K.M. Paraskevopoulos, M.G. Kanatzidis, Mat. Res. Soc. Symp. Proc. 691 (2002) 419–424.
[6] S.N. Dhar, C.F. Desai, Philos. Mag. Lett. 82 (2002) 581–587.
[7] A.V. Kuznetsov, S.D. Letyuchenko, V.V. Motskin, J. Thermoelectr. (2002) 43–48.
[8] T. Thonhauser, T.J. Scheidemantel, J.O. Sofo, J.V. Badding, G.D. Mahan, Phys. Rev. B 68 (2003) 085201/085201-085201/085208.
[9] E. Dashjav, A. Szczepenowska, H. Kleinke, J. Mater. Chem. 12 (2002) 345–349.

[10] N. Soheilnia, E. Dashjav, H. Kleinke, Can. J. Chem. 81 (2003) 1157–1163.
[11] M.G. Kanatzidis, T.J. McCarthy, T.A. Tanzer, L.-H. Chen, L. Iordanidis, T. Hogan, C.R. Kannewurf, C. Uher, B. Chen, Chem. Mater. 8 (1996) 1465–1474.
[12] D.-Y. Chung, T. Hogan, P. Brazis, M. Rocci-Lane, C. Kannewurf, M. Bastea, C. Uher, M.G. Kanatzidis, Science (Washington, DC). 287 (2000) 1024–1027.
[13] K.-F. Hsu, D.-Y. Chung, S. Lal, A. Mrotzek, T. Kyratsi, T. Hogan, M.G. Kanatzidis, J. Am. Chem. Soc. 124 (2002) 2410–2411.
[14] T. Kyratsi, J.S. Dyck, W. Chen, D.-Y. Chung, C. Uher, K.M. Paraskevopoulos, M.G. Kanatzidis, J. Appl. Phys. 92 (2002) 965–975.
[15] D.-Y. Chung, S. Jobic, T. Hogan, C.R. Kannewurf, R. Brec, J. Rouxel, M.G. Kanatzidis, J. Am. Chem. Soc. 119 (1997) 2505–2515.
[16] N.P. Blake, L. Mollnitz, G. Kresse, H. Metiu, J. Chem. Phys. 111 (1999) 3133–3144.
[17] F. Chen, K.L. Stokes, G.S. Nolas, J. Phys. Chem. Solids 63 (2002) 827–832.
[18] A. Bentien, B.B. Iversen, J.D. Bryan, G.D. Stucky, A.E.C. Palmqvist, A.J. Schultz, R.W. Henning, J. Appl. Phys. 91 (2002) 5694–5699.
[19] J. Kitagawa, T. Sasakawa, T. Suemitsu, T. Takabatake, M. Ishikawa, J. Phys. Soc. Japan 71 (2002) 1222–1225.
[20] E.A. Skrabek, D.S. Trimmer, in: D.M. Rowe (Ed.), CRC Handbook of Thermoelectrics, CRC Press, Boca Raton, FL, 1995, pp. 267–275.
[21] L.E. Shelimova, P.P. Konstantinov, O.G. Karpinsky, E.S. Avilov, M.A. Kretova, J.P. Fleurial, Int. Conf. Thermoelectr. 18 (1999) 536–540.
[22] R. Pocha, M. Tampier, R.D. Hofmann, B.D. Mosel, R. Pöttgen, D. Johrendt, Z. Anorg. Allg. Chem. 629 (2003) 1379–1384.
[23] P. Wu, J.A. Ibers, J. Solid State Chem. 107 (1993) 347–355.
[24] X. Jin, L. Zhang, G. Shu, R. Wang, H. Guo, J. Alloys Compd. 347 (2002) 67–71.
[25] D. Johrendt, M. Tampier, Chem. Eur. J. 6 (2000) 994–998.
[26] K.-S. Choi, J.A. Hanko, M.G. Kanatzidis, J. Solid State Chem. 147 (1999) 309–319.
[27] G.P. Voutsas, A.G. Papazoglou, P.J. Rentzeperis, Z. Kristallogr. 171 (1985) 261–268.
[28] K.-S. Choi, M.G. Kanatzidis, Inorg. Chem. 40 (2001) 101–104.
[29] SAINT. Version 4 ed. Siemens Analytical X-ray Instruments Inc., Madison, WI, 1995.
[30] G. M. Sheldrick. SHELXTL. Version 5.12 ed. Siemens Analytical X-ray Systems, Madison, WI, 1995.
[31] O.K. Andersen, Phys. Rev. B 12 (1975) 3060–3083.
[32] H.L. Skriver, The LMTO Method, Springer, Berlin, Germany, 1984.
[33] L. Hedin, B.I. Lundqvist, J. Phys. 4C (1971) 2064–2083.
[34] P.E. Blöchl, O. Jepsen, O.K. Andersen, Phys. Rev. B 49 (1994) 16223–16233.
[35] R. Dronskowski, P.E. Blöchl, J. Phys. Chem. 97 (1993) 8617–8624.
[36] T. Hughbanks, R. Hoffmann, J. Am. Chem. Soc. 105 (1983) 3528–3537.
[37] R.S. Mulliken, J. Chem. Phys. 23 (1955) 2343–2346.
[38] C.-S. Lee, H. Kleinke, Eur. J. Inorg. Chem. (2002) 591–596.
[39] I. Elder, C.-S. Lee, H. Kleinke, Inorg. Chem. 41 (2002) 538–545.
[40] E. Dashjav, H. Kleinke, J. Solid State Chem. 176 (2003) 329–337.
[41] L. Pauling, The Nature of the Chemical Bond, 3rd Edition, Cornell University Press, Ithaca, NY, 1948.
[42] G. Dittmar, H. Schäfer, Acta Crystallogr. B 32 (1976) 2726–2728.
[43] K. Nassau, The Physics and Chemistry of Color, 2nd Edition, Wiley, New York City, NY, USA, 2001.
[44] H. Yanagi, S.-I. Inoue, K. Ueda, H. Kawazoe, J. Appl. Phys. 88 (2000) 4159–4163.
[45] M. Tampier, D. Johrendt, Z. Anorg. Allg. Chem. 627 (2001) 312–320.